Inorganic Chemistry

ARTICLE

pubs.acs.org/IC

Magnetic Properties after Irradiation of 1:4 Complexes Consisting of CoX_2, X = NCS^-, Cl^-, and NCO^-, and Phenylpyridyldiazomethane in Dilute Frozen Solutions: Axial Ligand Effect in Heterospin Single-Molecule Magnets

Satoru Karasawa and Noboru Koga*

Graduate School of Pharmaceutical Sciences, Kyushu University, 3-1-1 Maidashi, Higashi-ku, Fukuoka 812-8582, Japan

Supporting Information

ABSTRACT: The solutions of 1:4 complexes of $Co(X)_2(\mathbf{D1py})_4$, X = Cl^-, and NCO^- and **D1py** = phenylpyridyldiazomethane, were photolyzed under cryogenic conditions, and their magnetic properties were investigated by direct current (DC) and alternating current (AC) magneto/susceptometries. After irradiation, the resulting cobalt-carbene complexes, $Co(X)_2(\mathbf{C1py})_4$, exhibited the behaviors of heterospin single-molecule magnets (SMMs) strongly depending on the axial ligands. In $Co(X)_2(\mathbf{C1py})_4$: X = Cl^- and NCO^-, the effective activation barriers, U_{eff}, for the reorientation of the magnetic moment and the resonant quantum tunneling time, τ_Q, characteristic to SMM properties were estimated to be 91 and 130 K, and 4×10^3 and 2×10^5 s, respectively. The τ_Q of $Co(NCS)_2(\mathbf{C1py})_4$ with U_{eff} = 89 K was found to be 6×10^2 s. In $Co(X)_2(\mathbf{C1py})_4$: X = Cl^- and NCO^-, temperature-dependent hysteresis loops were also observed below the blocking temperature (T_B = 3.2 and 4.8 K, respectively) and the coercive forces, H_c, of 7.0 and 20 kOe at 1.9 K, respectively, were obtained. In a series of 1:4 complexes of $Co(X)_2(\mathbf{C1py})_4$, X = NCS^-, Cl^-, and NCO^-, the axial ligands strongly affected the heterospin SMM properties, and the NCO^- ion having the large magnitude of the ligand-field splitting in a spectrochemical series, gave the largest U_{eff} and H_c and the longest τ_Q.

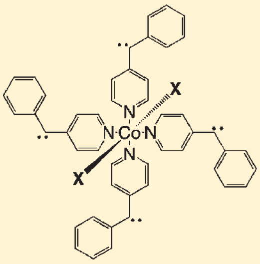

Heterospin Single-molecule Magnets

	U_{eff}/K	τ_Q/sec	H_c/kOe	T_B/K
X = NCS^-	89	6×10^2	7.0	3.2
= Cl^-	91	4×10^3	7.0	3.2
= NCO^-	130	2×10^5	20	4.8

INTRODUCTION

The single-molecule magnet (SMM)[1−4] exhibits a slow magnetic relaxation at low temperature and shows a hysteresis loop of magnetization, which is a classical magnetic property for bulk magnets, at even lower temperatures (below the blocking temperature, T_B). In addition, the unique magnetic property of SMMs is a quantum tunneling of magnetization[1,4] observed in the magnetic relaxation process. From these unique magnetic properties, the metal complexes showing SMM behavior have been intensively explored and studied in the field of the molecule-based magnet. Furthermore, since SMMs have a size on the nanometer scale, their development and use as new functional nanomaterials and nanomagnetic materials are anticipated. The slow magnetic relaxation characteristic of SMM magnetic behavior takes place via two pathways. One is the pathway crossing the thermal potential energy (the thermodynamic activation barrier, U) from the up-spin (or down-spin) to the down-spin (or up-spin). A large U corresponding to $|D|S^2$, D (<0) is a zero-field splitting parameter and S is a spin quantum number, produces hysteresis of the magnetization below T_B. The other is the pathway due to the resonant quantum tunneling (RQT) effect related to the transverse interaction.[4] The activation barrier, U, for reorientation of the magnetism is affected by the RQT effect to reduce the effective activation barrier, U_{eff}; $U > U_{eff}$. To obtain an SMM with large U_{eff}, therefore, the molecule of a metal complex isolated magnetically should be required to have not only large S and $|D|$ values but also a small RQT effect.

Up to now, many uniaxis anisotropic complexes and clusters containing various kinds of $3d^{2-4}$ and $4f^{5,6}$ metal ions have been reported as SMMs. However, in most of them, the values of U_{eff} are small (<30 K) except for a Mn_{12} family[2a−c,4b,4c] and lanthanide complexes.[6] The construction of an SMM with a large U_{eff} value or a high T_B thus becomes an interesting and challenging target in the field of the molecule-based magnets. For the construction of SMMs, we proposed the use of a heterospin system[7−9] consisting of the 3d spins of the metal ions and the 2p spins of the organic radicals and successfully observed SMM behaviors with large U_{eff} values (>30 K). In the heterospin systems,[7−11] any combination of the anisotropic metal ion and the organic spin may be used for SMMs. The simple 1:4 cobalt(II) complexes, $[Co(NCS)_2(\mathbf{C1py})_4]$[8a] and $[Co(NCO)_2(\mathbf{4NOpy})_4]$,[8b] in which carbene and aminoxyl, respectively, were used as organic spin sources, functioned as SMMs with relatively large U_{eff} values of 89 and 50 K, respectively, in frozen solution. The formation of a heterospin SMM in frozen solution was confirmed by a single-crystal study of cobalt-aminoxyl complex in which the aminoxyl centers were blocked by bulky *tert*-butyl groups to avoid the intermolecular magnetic interaction. The 1:4 Co(II)

Received: March 8, 2011
Published: April 26, 2011

complex[9f], $[Co(NCO)_2(\mathbf{TBPNOpy})_4]$, behaved as an SMM with U_{eff} = 28 K in a crystalline state and with U_{eff} = 48 K in a frozen solution. In addition, we found that the cyclic 2:2 Co-diazo complex[9g], $[Co(\textit{tert}\text{-Bu-hfpip})_2(\mathbf{D2py_2})]_2$, hfpip =1, 1, 1, 5, 5, 5-hexafluoro-4-(4-*tert*- butylphenylimino)-2-pentanonate, was photolyzable in the solid state, and the corresponding Co-carbene complex generated by photolysis in the crystalline state showed heterospin SMM behavior with U_{eff} = 91 K.

To improve and develop the carbene-cobalt system in heterospin SMM, this time, the axial ligand effects on the magnetic properties of the 1:4 complexes, $[Co(X)_2(\mathbf{C1py})_4]$, where X is a counterion at the axial ligands, were investigated by varying the axial ligands systematically in frozen solution. The ions NCS^-, Cl^-, and NCO^-, in which the magnitude of the ligand field splitting in a spectrochemical series is in the order of $NCS^- < Cl^- < NCO^-$,[12] were selected as axial ligands. In the aminoxyl-cobalt system, the axial ligand effect on the U_{eff} values has been already investigated, and $Co(X)_2(\mathbf{4NOpy})_4$, X = Br^-, NCS^-, and, NCO^-, were reported to have U_{eff} of 20, 31, and 50 K, respectively.[9c] In the carbene-cobalt system as well as the aminoxyl-cobalt system, the change of the axial ligand might affect the heterospin SMM property. The comparison of the U_{eff} value (89 K) for $Co(NCS)_2(\mathbf{C1py})_4$ with that (31 K) for $Co(NCS)_2(\mathbf{4NOpy})_4$ suggested the formation of SMM complexes with a large activation barrier for the reorientation of the magnetic moment in the carbene-cobalt system. Especially, $Co(NCO)_2(\mathbf{C1py})_4$ ligating with NCO^- as the axial ligand was expected to have a U_{eff} value larger than 89 K. In this study, indeed, $Co(NCO)_2(\mathbf{C1py})_4$ gave the U_{eff} value of 130 K, which is the largest among the heterospin SMMs. Furthermore, temperature-independent direct current (DC) magnetization decays because of the resonant quantum tunneling time, τ_Q, were observed in the range of 3.0−1.9 K and the τ_Q value was found to depend on the axial ligand. We will report here the axial-ligand dependence on the U_{eff} and τ_Q of the heterospin SMM properties in $Co(X)_2(\mathbf{C1py})_4$, X = NCS^-, Cl^-, and NCO^-.

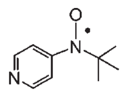

4NOpy

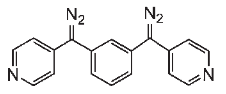

D2py2

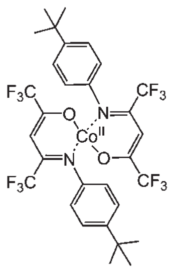

Co(*tert*-Buhfpip)2

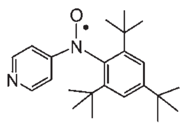

TBPNOpy

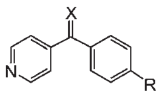

X = N_2 or • •

D1py; R = H, X = N_2
C1py; R = H, X = • •
D1py'; R = *tert*-Bu, X = N_2
C1py'; R = *tert*-Bu, X = • •

EXPERIMENTAL SECTION

General Procedures. Infrared spectra were recorded on a JASCO 420 FT-IR spectrometer. ^1H NMR spectra were measured on a JEOL 270 using $CDCl_3$ as the solvent and referenced to TMS. Mass spectra were measured on a JEOL JMS-600HMS spectrometer. Melting points were obtained with a MEL-TEMP heating block and are uncorrected. Elemental analyses were performed in the Analytical Center of the Faculty of Science in Kyushu University.

Visible-Near Infrared Spectra Measurements at Cryogenic Temperature. Visible-near-infrared spectra were recorded on a JASCO V570 spectrometer attached with an NACC cryo-system LTS-22X for the low temperature measurements. The solution samples were placed in separable quartz cells (path length; 1 mm) under a helium atmosphere. Photolyses of diazo samples were performed by argon ion laser (514 nm, 200 mW, Omnichrome 543−200M).

Table 1. Crystallographic Data of $[Co(Cl)_2(\mathbf{D1py'})_4]$ and $[Co(NCO)_2(\mathbf{D1py})_4]$

	$[Co(Cl)_2(\mathbf{D1py'})_4]$	$[Co(NCO)_2(\mathbf{D1py})_4]$
empirical formula	$C_{64}H_{68}N_{12}Cl_2Co$	$C_{50}H_{36}N_{14}O_2Co$
fw	1141.96	925.87
crystal system	orthorhombic	monoclinic
space group	*Pbcn* (no. 60)	*P*21/*n* (no. 14)
a (Å)	11.6865(10)	10.125(12)
b (Å)	22.1370(19)	11.394(16)
c (Å)	23.058(2)	19.725(19)
β (deg)	90	105.36(4)
V ($Å^3$)	5965.2(9)	2194(5)
Z	4	2
crystal size (mm)	0.30 × 0.30 × 0.10	0.40 × 0.40 × 0.30
D_{calc} (g cm^{-3})	1.271	1.401
color	red	red
F(000)	2352	954
radiation	Mo−Kα	Mo−Kα
R_1, wR_2 $[I > 2\sigma(I)]$[a]	0.079, 0.225	0.055, 0.120
GOF	0.910	1.133
no of obs.	10352	4082
no of variables	392	469

[a] $R_1 = \Sigma||F_o| - |F_c||/\Sigma|F_o|$; $wR_2 = \{\Sigma w(F_o^2 - F_c^2)^2/\Sigma w(F_o^2)^2\}^{1/2}$.

X-ray Crystal and Molecular Structure Analyses. Crystallographic data and experimental details for $[Co(Cl)_2(\mathbf{D1py'})_4]$ and $[Co(NCO)_2(\mathbf{D1py})_4]$ are summarized in Table 1. Suitable single crystals were glued onto a glass fiber using epoxy resin. All X-ray data were collected on a Rigaku Raxis-Rapid diffractometer with graphite monochromated MoK_a radiation (λ = 0.71069 Å). Reflections were collected at 123 ± 1 K. The molecular structures were solved by direct methods (SIR program[13]). The refinements were converged using the full-matrix least-squares method from the Crystal Structure software package[14] to give the *Pbcn* (no. 60) for $[Co(Cl)_2(\mathbf{D1py'})_4]$ and *P*21/*n* (no. 14) for $[Co(NCO)_2(\mathbf{D1py})_4]$. All non-hydrogen atoms were refined anisotropically. Hydrogen atoms were included at standard positions (C−H = 0.96 Å, C−C−H = 120°) and refined isotropically using a rigid model. Crystallographic data for the structure reported in this paper have been deposited with the Cambridge Crystallographic Data Center as supplementary publications nos. CCDC-809474 and -809469 for $[Co(Cl)_2(\mathbf{D1py'})_4]$ and $[Co(NCO)_2(\mathbf{D1py})_4]$, respectively.

Magnetic Measurements. Alternating current (AC) and DC magnetic susceptibility data were obtained on Quantum Design MPMS2 (0 ∼ ± 10 kOe) and MPMS-5S (0 ∼ ± 50 kOe) SQUID magneto/susceptometers, respectively.

(A). Preparation of Solution Samples. Solutions (5 or 10 mM) of the samples for the SQUID measurements were obtained by two methods, A and B, as follows. Method A: a solution (1 mL) of $Co(Cl^-$ and $NCS^-)_2$ (20 mmol) in 2-methyltetrahydrofuran (MTHF) and a solution (1 mL) of **D1py** (80 mmol) in MTHF were mixed and used as samples. Method B: a solution of crystal dissolved in MTHF was used as the sample. Method A was used for the measurements of $Co(Cl)_2(\mathbf{D1py})_4$, while method B was used for $[Co(NCO)_2(\mathbf{D1py})_4]$ and $[Co(Cl)_2(\mathbf{D1py'})_4]$. It was confirmed that there was no difference in the

magnetic data of the samples of [Co(NCS)$_2$(**D1py**)$_4$] and [Co(Cl)$_2$(**D1py′**)$_4$], which were obtained as crystals, prepared by Methods A and B. Furthermore, no concentration effect on the magnetic behavior in the concentration range examined was confirmed by the comparison of the magnetic data for 2.5, 5, and 10 mM samples of Co(Cl)$_2$(**D1py**)$_4$.

(B). General Procedure for SQUID Measurement in Frozen Solution. The solution sample was lightly degassed by bubbling nitrogen gas, and 50 μL of sample solution was placed into the capsule with a microsyringe. The capsule was attached to a handmade SQUID sample rod for the photolysis by a straw. The AC and DC magnetic susceptibility measurements were performed in the temperature range of 1.9−15 and 1.9−20 K, respectively, before and after irradiation. The irradiation system was reported previously.[7] Before irradiation, the $\chi_{\mathrm{mol}}T$ values for all samples in the range of 1.9−20 K were nearly constant at about 1.9−2.1 cm^3 K mol^{-1} for Co(Cl)$_2$(**D1py**)$_4$ and Co(NCO)$_2$(**D1py**)$_4$, respectively. The magnetic susceptibility of the MTHF solution itself was measured under similar conditions and was used as the control data.

The samples were taken out of the apparatus after SQUID measurements and were measured by IR spectra on KBr pellets. The quantitative photolyses of the samples were confirmed by the difference of the absorption due to the diazo moiety (~2050 cm^{-1}) before and after irradiation.

Materials. MTHF and ether were distilled from sodium benzophenone ketyl. **D1py** and [Co(NCS)$_2$(**D1py**)$_4$] were prepared by the procedure reported previously.[8a]

*4-tert-Butyl-(4-pyridil(diazo)methyl)benzene, **D1Py′**.* This was prepared in a manner similar to the procedure for **D1py** by using the corresponding ketone in place of 4-benzoylpyridine. Mp (decomp.) 118−120 °C, IR (KBr pellet) 2043 (C═N$_2$) cm^{-1}, UV−vis (CH$_2$Cl$_2$; ε) 304 (12012) and 495 (121) nm, Mass spectrum (Fab, *m*-nitrobenzyl alcohol matrix) m/z 252 (M$^+$1), ^{1}H NMR (CDCl$_3$, 270 MHz) δ 8.43 (d, J = 7.1 Hz, 2H), 7.35−7.26 (m, 6H), 1.35 (s, 9H). Anal. Calcd for $C_{16}H_{17}N_3$: C, 76.46; H, 6.82; N, 16.72. Found: C, 76.76; H, 6.52; N, 16.49

*Tetrakis[4-(phenyldiazomethyl)pyridine]di(isocyanato-N)cobalt(II), [Co(NCO)$_2$(**D1py**)$_4$].* A solution of Co(NO$_3$)$_2$ 6H$_2$O (37 mg, 0.13 mmol) in EtOH (5 mL) and KNCO (42 mg, 0.52 mmol) in H$_2$O (0.5 mL) was mixed with a solution of **D1py** (100 mg, 0.51 mmol) in CH$_2$Cl$_2$ (5 mL). *n*-Hexane (5 mL) was added to the mixture, and the resulting precipitates were removed by filtration. The solution was kept at −14 °C. The complex, [Co(NCO)$_2$(**D1py**)$_4$], was obtained as dark red brick-like crystals (20 mg). mp (dec.) 80−82 °C, IR (KBr pellet) ν = 2200 (NCO) and 2054 (C═N$_2$) cm^{-1}; Anal. Calcd for $C_{50}H_{36}N_{14}O_2Co$: C 65.00, H 3.93, N 21.23%; found: C 65.23, H 3.99, N 21.01%.

*Tetrakis[4-(4-tert-butylphenyldiazomethyl)pyridine]di(chloride)cobalt(II), [Co(Cl)$_2$(**D1py′**)$_4$].* This was prepared in a manner similar to the procedure for [Co(NCS)$_2$(**D1py**)$_4$] by using CoCl$_2$6H$_2$O and **D1py′** in place of Co(NCS)$_2$ and **D1py**, respectively. [Co(Cl)$_2$(**D1py′**)$_4$] was crystallized from *n*-hexane/CH$_2$Cl$_2$ to afford dark red brick-like crystals. Mp (decomp.) 103−105 °C, IR (KBr) 2051 (C = N$_2$) cm^{-1}, Anal. Calcd. for $C_{64}H_{68}N_{12}Cl_2Co$: C, 67.72; H, 6.04; N, 14.81. Found: C, 67.92; H, 6.00; N, 14.64.

■ RESULTS AND DISCUSSION

Preparation. The 1:4 cobalt(II) complexes, CoX$_2$(**D1py**)$_4$, X = NCS$^-$ and Cl$^-$, were prepared by mixing the solution of CoX$_2$ in EtOH or MTHF with the solution of **D1py** in MTHF at 1 to 4 ratios. In the preparation of [Co(NCO)$_2$(**D1py**)$_4$], a 1:2 mixture of Co(NO$_3$)$_2$ and KNCO was used without isolation of Co(NCO)$_2$. [Co(NCO)$_2$(**D1py**)$_4$] and [Co(NCS)$_2$(**D1py**)$_4$] were crystallized from CH$_2$Cl$_2$/*n*-hexane to afford red brick-like crystals, while [Co(Cl)$_2$(**D1py**)$_4$] was obtained only as a powder. In contrast, [Co(Cl)$_2$(**D1py′**)$_4$], where **D1py′** has a *tert*-buyl group at the 4-position of the phenyl ring, was obtained as red brick-like crystals. **D1py′** was prepared by a procedure similar to that for **D1py**.[8a]

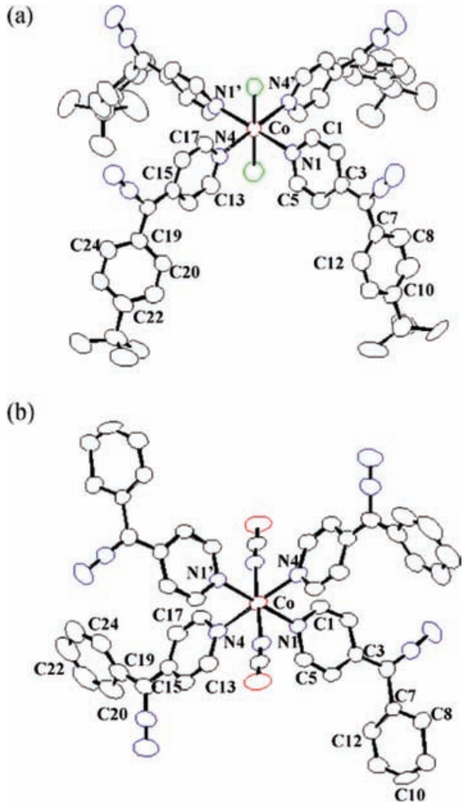

Figure 1. ORTEP drawings of the molecular structure of (a) [Co(Cl)$_2$(**D1py′**)$_4$] and (b)[Co(NCO)$_2$(**D1py**)$_4$] (C; black, N; blue, O; red, Cl; green, and Co; pink). Hydrogen atoms and the disorder parts are omitted for the sake of clarity.

*X-ray Molecular Structure Analyses of [Co(Cl)$_2$(**D1py′**)$_4$] and [Co(NCO)$_2$(**D1py**)$_4$].* The single crystals of [Co(NCO)$_2$(**D1py**)$_4$] and [Co(Cl)$_2$(**D1py′**)$_4$] were analyzed by X-ray crystallography. Both complexes had similar hexa-coordinated structures, in which each cobalt ion is surrounded with four nitrogen atoms of the pyridine rings (N$_{\mathrm{Py}}$) at the basal plane and two counterions at the apical positions. [Co(NCO)$_2$(**D1py**)$_4$] has a disorder at the phenyldiazomethyl position in an occupancy ratio of 0.63 and 0.37. The molecular geometry for [Co(NCO)$_2$(**D1py**)$_4$] is a compressed octahedron with a center of symmetry at the cobalt ion, which is similar to that for [Co(NCS)$_2$(**D1py**)$_4$]. In contrast, the molecular geometry for [Co(Cl)$_2$(**D1py′**)$_4$] is an elongated octahedron without a center of symmetry at the cobalt ion. Elongation of the bond length of Co-halide was also observed in [Co(Br)$_2$(**4NOpy**)$_4$][9c] as reported previously. ORTEP drawings of the molecular structures of [Co(Cl)$_2$(**D1py′**)$_4$] and [Co(NCO)$_2$(**D1py**)$_4$] are shown in Figure 1.

In the octahedral structure, the bond lengths ($r_{\mathrm{Co-N(NCO)}}$) between the axial ligand and the cobalt ion for [Co(NCO)$_2$(**D1py**)$_4$] are shorter by 0.086−0.129 Å compared with those ($r_{\mathrm{Co-N(Py)}}$) between the nitrogen of pyridine and the cobalt ion: $r_{\mathrm{Co-N(NCO)}}$ = 2.092 and $r_{\mathrm{Co-N(Py)}}$ = 2.178 and 2.221 Å, while those for [Co(Cl)$_2$(**D1py′**)$_4$] are longer by 0.233−0.437 Å; $r_{\mathrm{Co-Cl}}$ = 2.464 and 2.508 Å and $r_{\mathrm{Co-N(Py)}}$ = 2.171, and 2.231 Å. The compressed octahedral structure for [Co(NCO)$_2$(**D1py**)$_4$]

Table 2. Selected Bond Lengths (Å) and Dihedral Angles (deg) for [Co(Cl)$_2$(D1py′)$_4$], [Co(NCO)$_2$(D1py)$_4$], and [Co(NCS)$_2$(D1py)$_4$]

	[Co(Cl)$_2$(**D1py′**)$_4$]	[Co(NCO)$_2$(**D1py**)$_4$]	[Co(NCS)$_2$(**D1py**)$_4$][a]
	Bond Lengths (Å)		
Co−N$_{py}$	2.171, 2.231	2.178, 2.221	2.162, 2.187
Co-Axial ligand	2.464, 2.508	2.092	2.092
	Dihedral Angles (deg) between Pyridine Ring and XY Plane		
N(1)N(4)N(1′)N(4′)−N(1)C(1)C(3) C(5)	67.21	60.09	58.34
N(1)N(4)N(1′)N(4′)−N(4)C(13)C(15)C(17)	82.96	84.40	75.83
	Dihedral Angles (deg) between Pyridine Ring and Phenyl Ring		
N(1)C(1)C(3) C(5)−C(7)C(8)C(10)C(11)	51.64	59.44	45.05
N(4)C(13)C(15)C(17)−C(19)C(20)C(22)C(24)	81.34	65.08	60.76

[a] Reference 8a.

is similar to that for [Co(NCS)$_2$(**D1py**)$_4$] reported previously.[8a] The linear axial ligands of NCO are coordinated to the cobalt ion by tilting angle (N$_{Py}$−Co−N$_{NCO}$) of 88.91°. The bond angles of C−C$_{N2}$−C and the dihedral angles between the pyridine and phenyl rings for the **D1py** units in both complexes are close to that (126.9 and 128.2°, respectively) for the metal free ligand, **D1py**. The dihedral angles between the pyridine ring and the XY plane defined by the nitrogen atoms of four pyridines are 60.09 and 84.40° for [Co(NCO)$_2$(**D1py**)$_4$] and 67.21 and 82.96° for [Co(Cl)$_2$(**D1py′**)$_4$]. The selected bond lengths, angles, and dihedral angles for [Co(Cl)$_2$(**D1py′**)$_4$] and [Co(NCO)$_2$(**D1py**)$_4$] are listed in Table 2 together with those for [Co(NCS)$_2$(**D1py**)$_4$].

*Visible and Near-Infrared (NIR) Spectra of CoX$_2$(**D1py**)$_4$, X = Cl$^-$ and NCO$^-$, and Co(Cl)$_2$(**D1py′**)$_4$.* To determine the coordination structure of the complexes formed in frozen solutions, Vis-NIR spectra of 1:4 mixtures (2.5 mM) of CoCl$_2$ and **D1py** in MTHF and the solution of [Co(NCO)$_2$(**D1py**)$_4$] and [Co(Cl)$_2$(**D1py′**)$_4$] dissolved in MTHF were measured in the temperature range 293−150 K. The temperature dependency of Vis-NIR spectra for the 1:4 mixture of CoCl$_2$ and **D1Py** in MTHF is shown in Figure 2a. The spectrum at room temperature showed two sets of absorptions at 580, 612, 642 (sh), 669 (sh), and 1025 nm and at 495 nm. The former and the latter absorptions are characteristic of the d-d transitions of cobalt(II) ion in the tetrahedral and octahedral structures, respectively.[16] In the latter absorption, the one at 495 nm ($\varepsilon = \sim 100$) due to $n-\pi^*$ transition for the diazo moieties of **D1py** was overlapped. On cooling to 200 K, absorptions for the former gradually decreased, while the latter at 495 nm increased (Figure 2a). At 150 K, the former absorptions disappeared completely. The observed spectrum changes indicate that the tetrahedral and octahedral species are equilibrated; the former is dominant at room temperature and the latter at temperatures below 200 K. Observed thermal-spectra changes on cooling suggest that the complex formed from the 1:4 mixture in frozen solution can safely be considered to be octahedral as observed in X-ray crystallography. Subsequently, the solution of the sample was cooled down to 12 K and was irradiated by an argon laser (λ = 514 nm) through an optical fiber. A new absorption at 460 nm appeared on photolysis, as shown in Figure 2b. In photolysis, the expense of diazo moieties was not clear because of the absorption at 495 nm due to the d-d transition of the octahedral cobalt ion. An absorption at 460 nm disappeared after the cycle of annealing at 100 K and cooling at 12 K, suggesting that it might be a characteristic absorption due to the $\pi-\pi^*$ transition for carbene. In fact, in the photolysis of **D1py** under similar condition, the absorption at 447 nm appeared with the expense of the one at 493 nm of diazo moiety (Supporting Information, Figure S1). The observed spectrum change of the 1:4 cobalt complex on photolysis was similar to that for the corresponding copper complex reported previously.[15] The spectra for the solutions of [Co(NCO)$_2$(**D1py**)$_4$] and [Co(Cl)$_2$(**D1py′**)$_4$] dissolved in MTHF also showed similar changes on cooling and on photolysis at 12 K.

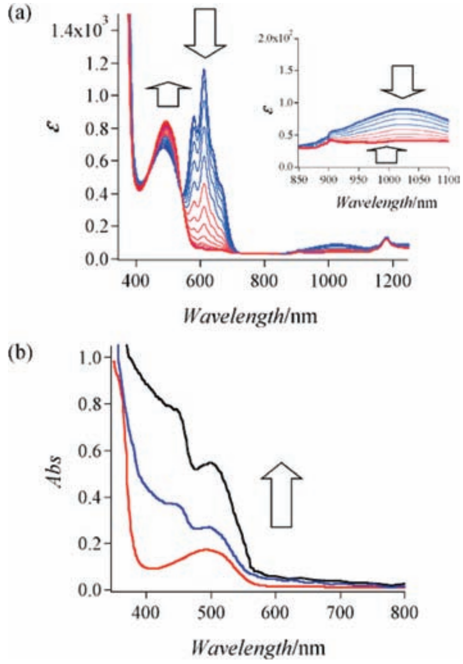

Figure 2. Vis-NIR spectral changes of a 1:4 mixture of CoCl$_2$ and **D1py** in MTHF solution (a) on cooling in the temperature ranges of 293−230 (blue) and 225−150 (red) K and (b) on photolysis (irradiation time for 0; red, 20; blue, and 60 min; black) at 12 K. Arrows indicate increase or decrease. The inset in (a) shows the spectra changes expanded in the long wavelength region.

Magnetic Properties. The solutions (10 mM, 50 μL) of the 1:4 mixture of CoCl$_2$ and **D1py** in MTHF and of the crystal of

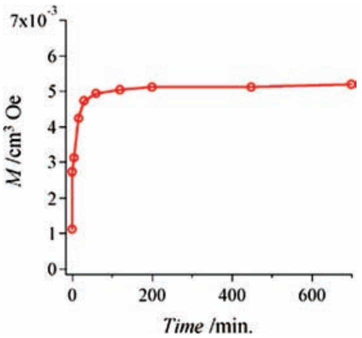

Figure 3. Plot of M versus irradiation time for the solution sample of $Co(Cl)_2(\mathbf{D1py})_4$ at 5 kOe at 5 K.

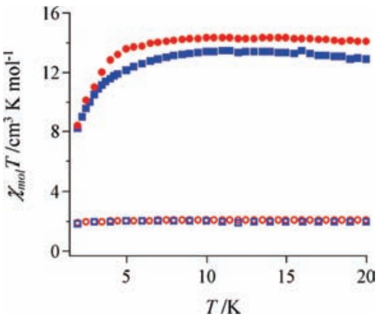

Figure 4. $\chi_{mol}T$ vs T plots before (open) and after (filled) irradiation of $Co(X)_2(\mathbf{D1py})_4$, X = Cl^- (square), and NCO^- (circle), below 20 K.

$[Co(NCO)_2(\mathbf{D1py})_4]$ dissolved in MTHF were employed as samples for SQUID measurements. DC and AC magnetic susceptibilities for all solution samples, $Co(X)_2(\mathbf{D1py})_4$, X = Cl^- and NCO^-, were measured after irradiation. To confirm no preparation dependence of the sample for $Co(X)_2(\mathbf{D1py})_4$, a solution of the crystal of $Co(Cl)_2(\mathbf{D1py'})_4$ dissolved in MTHF was also used as a sample, and DC and AC magnetic measurements were carried out.

Photolyses of $CoX_2(\mathbf{D1py})_4$, X = Cl^- and NCO^-, and $Co(Cl)_2(\mathbf{D1py'})_4$ in Frozen Solution. Photolyses of the solution samples were performed in a SQUID apparatus through an optical fiber[7] and followed by magnetization (M) measurements at 5 kOe at 5 K. The M versus irradiation time plot for the solution sample of $Co(Cl)_2(\mathbf{D1py})_4$ is shown in Figure 3. When the irradiation commenced, the M values gradually developed and leveled off after about 2 h. The increase in the M values on photolysis indicates the generation of triplet carbene.

In the AC and DC measurements under similar conditions after annealing at 100 K, the magnetic behavior observed after irradiation completely disappeared and reverted to that before irradiation. Furthermore, the quantitative photolysis of the sample was confirmed by the disappearance of the absorption at about 2050 cm^{-1} due to the diazo moiety in the IR spectra after SQUID measurements.

DC Magnetic Susceptibility Measurements. *(A). Temperature Dependence of DC Magnetic Susceptibilities.* The values of DC molar magnetic susceptibility, χ_{mol}, before and after irradiation of $Co(X)_2(\mathbf{D1py})_4$, X = Cl^- and NCO^-, and $Co(Cl)_2(\mathbf{D1py'})_4$ in frozen solution were collected at a constant field of 5 kOe below 20 K. The obtained χ_{mol} values were plotted as a function of temperature. The plots of $\chi_{mol}T$ versus T for $Co(X)_2(\mathbf{C1py})_2$, X = Cl^- and NCO^-, before and after irradiation are shown in Figure 4 and that for $Co(Cl)_2(\mathbf{D1py'})_4$ is shown in Supporting Information, Figure S2.

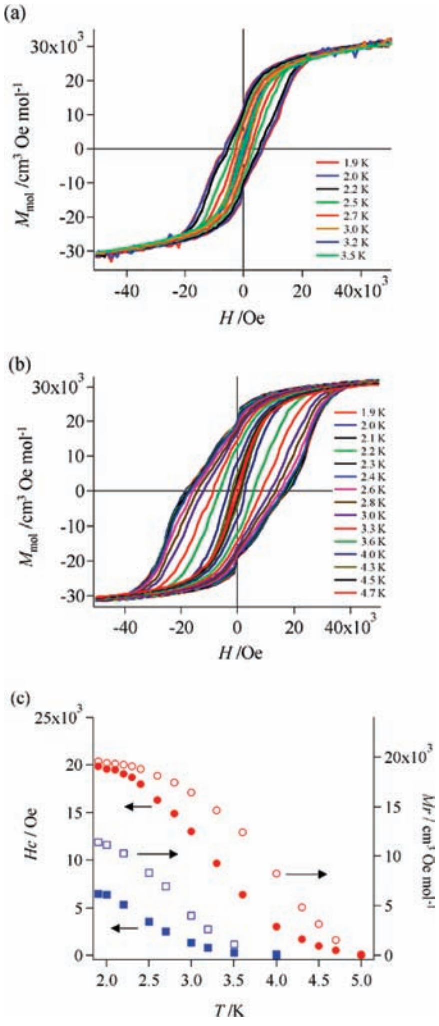

Figure 5. Plots of M_{mol} vs H for (a) $Co(Cl)_2(\mathbf{C1py})_4$ and (b) $Co(NCO)_2(\mathbf{C1py})_4$ at given temperatures in frozen MTHF solution with a sweep rate of 0.35 kOe/sec and (c) H_c (filled) and M_r (open) vs T plots for $Co(Cl)_2(\mathbf{C1py})_4$ (square) and $Co(NCO)_2(\mathbf{C1py})_4$ (circle).

Before irradiation, the $\chi_{mol}T$ values for three samples were comparable and were nearly constant (2.0 cm^3 K mol^{-1}) in the temperature range of 1.9−20 K. The constant value of 2.0 cm^3 K mol^{-1} was consistent with that for octahedral $Co(X)_2(\mathbf{py})_4$ reported previously.[17] After irradiation, the $\chi_{mol}T$ values increased greatly, and those at 20 K were 12.9 and 14.0 cm^3 K mol^{-1} for $Co(X)_2(\mathbf{C1py})_2$, X = Cl^-, and NCO^-, respectively. The values at 20 K were much larger than the theoretical values (6 cm^3 K mol^{-1}) calculated by a spin-only equation with two isolated high-spin carbenes (1.0 cm^3 K mol^{-1} × 4) and one high-spin cobalt(II) ion[17,18] with effective spin $S'_{eff} = 1/2$ ($\chi_{mol}T$ value of 2.0 cm^3 K mol^{-1} before irradiation), suggesting that the carbenes and the cobalt ions in the complex interacted ferromagnetically to form a high-spin ground state with $S_{total} = 9/2$. On cooling, the $\chi_{mol}T$ values were nearly constant for 10−20 K and gradually decreased at lower temperatures. The decrease in

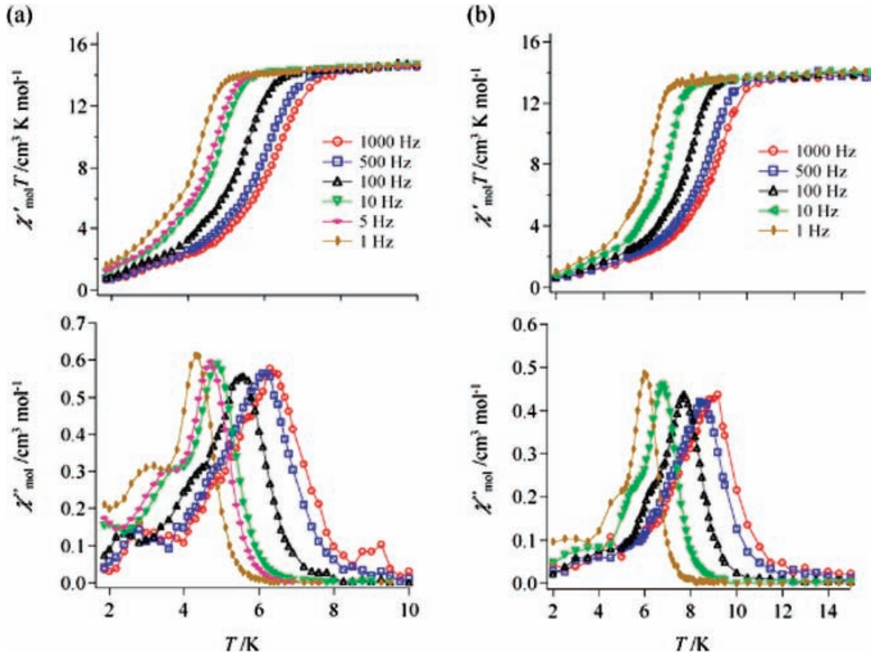

Figure 6. Plots of $\chi'_{mol}T$ vs T (upper) and χ''_{mol} vs T (lower) for $Co(Cl)_2(\mathbf{C1py})_4$ (a) and $Co(NCO)_2(\mathbf{C1py})_4$ (b) in frozen MTHF solution with a 5 Oe AC field oscillating at given frequencies. The solid lines are visual guides.

the $\chi_{mol}T$ values for both complexes below 5 K indicates an effect of the zero-field splitting caused by spin−orbit coupling in the cobalt ion.[12] The thermal profile of $\chi_{mol}T$ for $Co(Cl)_2(\mathbf{D1py'})_2$ was similar to that for $Co(Cl)_2(\mathbf{C1py})_4$.

(B). Hysteresis Loops for $Co(X)_2(\mathbf{C1py})_4$, X = Cl^- and NCO^-, and $Co(Cl)_2(\mathbf{C1py'})_4$. The DC magnetizations for $Co(X)_2(\mathbf{C1py})_4$, X = Cl^- and NCO^-, and $Co(Cl)_2(\mathbf{C1py'})_4$ were measured in the range −50 to 50 kOe with a field-sweep rate of 0.35 kOe/sec at various temperatures in the range 1.9−5.0 K. The M_{mol} values gradually increased on applying the field and continued to increase even at 50 kOe at which point the M_{mol} value were 3.1×10^4, 3.2×10^4, and 3.4×10^4 cm^3 Oe mol^{-1} for $Co(X)_2(\mathbf{C1py})_4$, X = Cl^- and NCO^-, and $Co(Cl)_2(\mathbf{C1py'})_4$, respectively. The values at 50 kOe were lower than those for the values of saturation magnetization, M_s, suggesting the effect of a large D. Furthermore, $Co(X)_2(\mathbf{C1py})_4$ and $Co(Cl)_2(\mathbf{C1py'})_4$ as well as $Co(NCS)_2(\mathbf{C1py})_4$ showed temperature-dependent hysteresis loops related with the field. The hysteresis loops appeared below about 3 and 5 K for $Co(X)_2(\mathbf{C1py})_4$ and $Co(Cl)_2(\mathbf{C1py'})_2$, respectively, and the width of the loop increased upon cooling. The hysteresis loops for $Co(X)_2(\mathbf{C1py})_4$, X = Cl^- and NCO^-, and $Co(Cl)_2(\mathbf{D1py'})_4$ at given temperatures are shown in Figure 5 and Supporting Information, Figure S3, respectively.

In $Co(X)_2(\mathbf{C1py})_4$, X = Cl^- and NCO^-, the values of H_c and M_r depended on the temperature. Both values were plotted as a function of temperature, as shown in Figure 5c. On cooling from 5.0 K, both values gradually increased until 2.0 K. The observed thermal profiles of H_c and M_r are characteristic of a SMM. The values of H_c and M_r at 1.9 K are 7.0 and 20 kOe and 1.1×10^4 and 2.0×10^4 cm^3 Oe mol^{-1} for $Co(X)_2(\mathbf{C1py})_4$, X = Cl^- and NCO^-, respectively. The corresponding values for $Co(Cl)_2(\mathbf{C1py'})_4$ were 7.0 kOe and 1.3×10^4 cm^3 Oe mol^{-1}, respectively, which were comparable with those for $Co(Cl)_2(\mathbf{C1py})_4$. In relation to the hysteresis loop, the H_c values depended on the axial ligand and increased in the order $Co(X)_2(\mathbf{C1py})_4$, X = NCS^-, Cl^-, and NCO^-. It is noted that the temperature at which H_c became constant is consistent with the one at which τ_Q was determined.

Magnetization Relaxations of $Co(X)_2(C1py)_4$, X = NCS^-, Cl^-, and NCO^-, and $Co(Cl)_2(C1py')_4$ in Frozen Solution. In SMMs, the characteristic slow magnetic relaxation for reorientation of the spins takes place via two pathways due to the thermal activation barrier and the resonant quantum tunneling (RQT).[4] The relaxations due to the former are temperature-dependent and obtained by the AC magnetic susceptibility technique, while those due to the latter are temperature-independent and determined by the temperature dependence of the DC magnetization decay at extremely low temperature. To investigate the axial ligand dependence of the SMM properties, the AC and DC magnetic susceptibilities for $Co(X)_2(\mathbf{C1py})_4$; **X** = NCS^-, Cl^-, and NCO^-, and $Co(Cl)_2(\mathbf{C1py'})_4$ were measured in frozen solutions.

(A). AC Magnetic Susceptibility Measurements of $Co(X)_2(\mathbf{C1py})_4$, X = Cl^- and NCO^-, and $Co(Cl)_2(\mathbf{C1py'})_4$ in Frozen Solution. AC magnetic susceptibility data for $Co(X)_2(\mathbf{C1py})_4$; **X** = NCS^-, Cl^-, and NCO^-, and $Co(Cl)_2(\mathbf{C1py'})_4$ were collected in a zero DC field with a 5.0 Oe AC field at the given frequencies in the range of 1000−1 Hz in the temperature range of 15−1.9 K. The results of $Co(NCS)_2(\mathbf{C1py})_4$ were reported previously.[8a]

In $Co(X)_2(\mathbf{C1py})_4$; **X** = Cl^- and NCO^-, and $Co(Cl)_2(\mathbf{C1py'})_4$, the χ'_{mol} and χ''_{mol} signals (in-phase and out-of-phase components of AC magnetic susceptibilities, respectively) and their frequency dependence were clearly observed, indicating that cobalt complexes have slow magnetic relaxations for reorientation of the magnetic moment. The maxima of χ''_{mol} signals for $Co(NCO)_2(\mathbf{C1py})_4$ compared with those for $Co(Cl)_2(\mathbf{C1py})_4$ at each frequency appeared at higher temperatures, suggesting that $Co(NCO)_2(\mathbf{C1py})_4$ has an anisotropic barrier larger than that for $Co(Cl)_2(\mathbf{C1py})_4$. The relative ratios

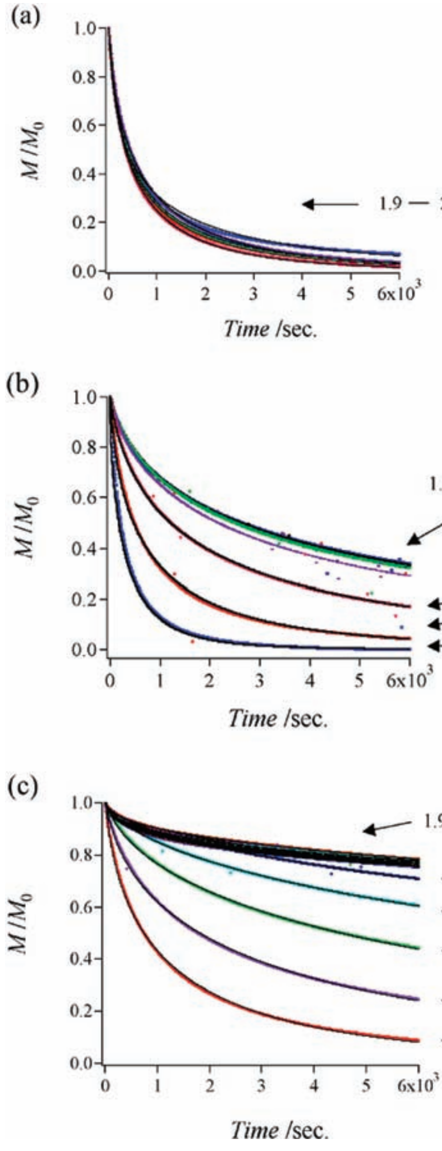

Figure 7. DC magnetization decays for 1:4 mixtures of (a) Co$(NCS)_2$(**C1py**)$_4$, (b) Co$(Cl)_2$(**C1py**)$_4$, and (c) Co$(NCO)_2$(**C1py**)$_4$ at given temperatures after applying a field of 50 and reducing to 0 kOe. Solid lines showed results fitted by the stretched exponential equation.

$(\chi''_{\mathrm{mol}}/\chi'_{\mathrm{mol}})$ of the χ''_{mol} and χ'_{mol} signal intensities were in the region of 0.3−0.4, which are consistent with the values for heterospin SMMs.[8] The plots of $\chi'_{\mathrm{mol}}T$ versus T and χ''_{mol} versus T for Co$(X)_2$(**D1py**)$_4$, X = Cl^- and NCO^-, and Co$(Cl)_2$(**C1py′**)$_4$ are shown in Figure 6 and Supporting Information, Figure S4, respectively.

In the plots of $\chi'_{\mathrm{mol}}T$ versus T for Co$(X)_2$(**C1py**)$_4$, X = Cl^- and NCO^-, and Co$(Cl)_2$(**C1py′**)$_4$, the values of $\chi'_{\mathrm{mol}}T$ at 15 K were 14.2, 14.0, and 14.1 cm^3 K mol^{-1}, respectively, and remained essentially constant on cooling until the onset of the contribution of χ''_{mol} signals. These constant values were consistent with those at 20 K in $\chi_{\mathrm{mol}}T$ versus T plots (Figure 4). Below 12 K, the $\chi'_{\mathrm{mol}}T$ values frequency-dependently decreased, while the χ''_{mol} signals appeared at the same temperature. The observed peak-top temperature of χ''_{mol} signals depended on the frequency, and it shifted to a higher temperature with increasing frequency.

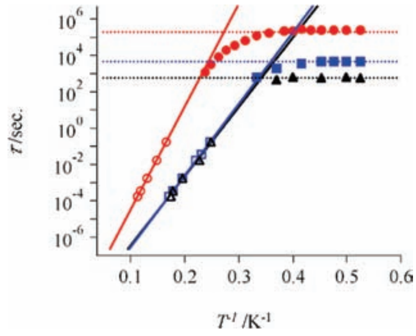

Figure 8. Plots of ln(τ) vs T^{-1} for Co$(NCS)_2$(**C1py**)$_4$ (black triangle), Co$(Cl)_2$(**C1py**)$_4$ (blue square), and Co$(NCO)_2$(**C1py**)$_4$ (red circle). The open and filled symbols indicate the data collected by the AC magnetic susceptibility technique and by DC magnetization decay, respectively. The solid lines are the least-squares fits of the data to the Arrhenius equation and the dotted lines indicate the τ_Q value.

The value of $\Delta T_f/T_f(0)\Delta(\log w)$, where ΔT_f is the shift of the peak-temperature in χ'_{mol}, log w is the logarithm of the applied frequency, and $T_f(0)$ is the position of the peak at zero frequency, was used for evaluation of the complexes showing slow magnetic relaxation. The values obtained from the χ'_{mol} versus T plots for Co$(X)_2$(**C1py**)$_4$, X = Cl^- and NCO^-, and Co$(Cl)_2$(**C1py′**)$_4$ were 0.25, 0.28, and 0.25, respectively. According to Mydosh's work,[19] those values are in the region $\Delta T_f/T_f(0)\Delta(\log w) > 0.2$ for a SMM and support the formation of a SMM rather than a spin glass.

*(B). DC Magnetization Decays of Co(X)$_2$(**C1Py**)$_4$, X = NCS$^-$, Cl$^-$, and NCO$^-$, and Co(Cl)$_2$(**C1py′**)$_4$ in Frozen Solution.* To characterize the slow magnetization relaxation at even lower temperatures, DC magnetization decay experiments for Co$(X)_2$(**C1py**)$_4$, X = Cl^- and NCO^- together with Co$(NCS)_2$(**C1py**)$_4$ were carried out below the temperature at which the hysteresis loop started to appear. The magnetization decays at 7 temperatures in the range 3.2−1.9 K, 9 in 3.5−1.9 K, and 19 in 4.8−1.9 K for Co$(X)_2$(**C1py**)$_4$, X = NCS^-, Cl^-, and NCO, respectively, were followed for 6000 s (Supporting Information, Figure S5). After the cycle of applying the outer field of 50 kOe at 10 K, cooling down to the desired temperature, and then reducing to 0 kOe, the magnetizations were measured as a function of time. It took about 120 s to reduce the field from 50 to 0 kOe. In Co$(NCS)_2$(**C1py**)$_4$, the experimental decays above 2.7 K were too fast to follow, while in Co$(NCO)_2$(**C1py**)$_4$, those below 3.0 K were slow and only 22% reduction of the magnitude of M_0 was observed after 6000 s. Taking into account the wasted time of about 120 s, the experimental decay data in the temperature range of 1.9−2.7, 1.9−3.0, and 1.9−4.2 K for Co$(X)_2$(**C1py**)$_4$, X = NCS^-, Cl^-, and NCO^-, were used. The values of magnetization at t = 0, M_0, were confirmed to be consistent with the values of M_r in the hysteresis loop at the given temperature. The magnetization data, M, were normalized by M_0 at each temperature, and the M/M_0 values were plotted as a function of time. The decay curves at given temperatures for Co$(X)_2$(**C1py**)$_4$, X = NCS^-, Cl^-, and NCO^-, and Co$(Cl)_2$(**C1py′**) are shown in Figure 7 and Supporting Information, Figure S6, respectively.

As observed in Figure 7, the magnetization decays depended on the complex, and the decay rate at the same temperature decreased in order of Co$(X)_2$(**C1py**)$_4$, X = NCS^-, Cl^-, and NCO^-. The decays also depended on the temperature and became slow on cooling. A noticeable point in the temperature

Table 3. Values of S_{total}, U_{eff}, τ_0, T_{B}, τ_{Q}, H_{c}, and M_{r}, for $\mathrm{Co(X)_2(\mathbf{C1py})_4}$, X = $\mathrm{NCS^-}$, $\mathrm{Cl^-}$, and $\mathrm{NCO^-}$, and $\mathrm{Co(Cl)_2(\mathbf{C1py'})_4}$ in MTHF Frozen Solution

complexes	S_{total}	U_{eff} (K)	τ_0 (sec)	T_{B} (K)[b]	τ_{Q} (sec)	H_{c} (kOe)	M_{r} (cm^3 Oe mol^{-1})
$\mathrm{Co(NCS)_2(\mathbf{C1py})_4}$[a]	9/2	89[a]	3.7×10^{-11}[a]	3.2	6×10^2	3.5[a]	7.6×10^3[a]
$\mathrm{Co(Cl)_2(\mathbf{C1py})_4}$	9/2	91	1.2×10^{-10}	3.2	4×10^3	7.0	1.1×10^4
$\mathrm{Co(Cl)_2(\mathbf{C1py'})_4}$	9/2	93	1.9×10^{-10}	3.3	5×10^3	7.0	1.3×10^4
$\mathrm{Co(NCO)_2(\mathbf{C1py})_4}$	9/2	130	6.8×10^{-11}	4.8	2×10^5	20	2.0×10^4

[a] Reference 8a. [b] Temperature at τ = 100 s in Arrhenius plot.

dependence of the decay was that the decays became independent of temperature below about 2.5, 2.7, and 3.0 K for $\mathrm{NCS^-}$, $\mathrm{Cl^-}$, and $\mathrm{NCO^-}$, respectively. This temperature-independent decay in the low temperature region indicated that the magnetization decay reached the spin quantum tunneling time, τ_{Q}. To investigate the magnetization decay quantitatively, the experimental data for $\mathrm{Co(X)_2(\mathbf{C1py})_4}$, X = $\mathrm{NCS^-}$, $\mathrm{Cl^-}$, and $\mathrm{NCO^-}$ were analyzed by means of the equation for a single-exponential decay and a stretched exponential decay.[20] First, the decay data were analyzed by a single-exponential decay to afford poor-fitting results. The data were then fitted to a stretched exponential decay (eq 1).[20]

$$\ln(M) = \ln(M_0) - (t/\tau)^B \qquad (1)$$

where M_0 is the initial magnetization, τ is the average relaxation time, and B is the width of the distribution; $B = 1$ is a single-exponential decay. The obtained τ values (B) were 4.4–5.4 × 10^2 (0.40–0.55), 0.6–4.5 × 10^3 (0.52–0.56), and 0.011–2.6 × 10^5 (0.3–0.59) sec for $\mathrm{Co(X)_2(\mathbf{C1py})_4}$, X = $\mathrm{NCS^-}$, $\mathrm{Cl^-}$, and $\mathrm{NCO^-}$, respectively. The values of the temperature-independent decay time were 6×10^2, 4×10^3, and 2×10^5 s for $\mathrm{Co(X)_2(\mathbf{C1py})_4}$, X = $\mathrm{NCS^-}$, $\mathrm{Cl^-}$, and $\mathrm{NCO^-}$, respectively. The values of τ and B obtained by a stretched exponential decay are listed in Supporting Information, Table S1, and the fitting curves are shown in Figure 7 as solid lines.

(C). Magnetization Relaxations in $\mathrm{Co(X)_2(\mathbf{C1py})_4}$, X = $\mathrm{NCS^-}$, $\mathrm{Cl^-}$, and $\mathrm{NCO^-}$, and $\mathrm{Co(Cl)_2(\mathbf{C1py'})_4}$. For $\mathrm{Co(X)_2(\mathbf{C1py})_4}$, X = $\mathrm{Cl^-}$ and $\mathrm{NCO^-}$, the data of DC magnetization decays were combined with those given by means of the AC magnetic susceptibility technique and were plotted as a function of inverse T. Similarly, the DC data for $\mathrm{Co(NCS)_2(\mathbf{C1py})_4}$ were combined with AC data reported previously and plotted. The $\ln(\tau)$ versus T^{-1} plots for $\mathrm{Co(X)_2(\mathbf{C1py})_4}$, X = $\mathrm{NCS^-}$, $\mathrm{Cl^-}$, and $\mathrm{NCO^-}$, and $\mathrm{Co(Cl)_2(\mathbf{C1py'})_4}$ are shown in Figure 8 and Supporting Information, Figure S7, respectively.

As observed in Figure 8, the relaxation times, τ, collected by the AC magnetic susceptibility technique and the DC magnetization decay measurements are clearly distinguishable. At higher temperatures, the decays obtained from the AC magnetic susceptibility experiments obey the Arrhenius law, $\tau = 1/(2\pi\nu) = \tau_0 \exp(U_{\mathrm{eff}}/k_{\mathrm{B}}T)$, which afford the kinetic activation barrier, $U_{\mathrm{eff}}/k_{\mathrm{B}}$, and the pre-exponential factor, τ_0. From the linear lines obtained by the least-squares fits of the data to the Arrhenius equation, the values of $U_{\mathrm{eff}}/k_{\mathrm{B}}$ and τ_0 were estimated to be 91 and 130 K and 3.1×10^{-9} and 1.2×10^{-10} s, for $\mathrm{Co(X)_2(\mathbf{C1py})_4}$, X = $\mathrm{Cl^-}$ and $\mathrm{NCO^-}$, respectively. The $U_{\mathrm{eff}}/k_{\mathrm{B}}$ and τ_0 values for $\mathrm{Co(Cl)_2(\mathbf{C1py'})_4}$ were 93 K and 1.9×10^{-10} s, respectively, which were close to those for $\mathrm{Co(Cl)_2(\mathbf{C1py})_4}$. In addition to the Mydosh values ($\Delta T_{\mathrm{f}}/T_{\mathrm{f}}(0)\Delta(\log w) = 0.25$ and 0.28 for $\mathrm{Co(X)_2(\mathbf{C1py})_4}$, X = $\mathrm{Cl^-}$ and $\mathrm{NCO^-}$, respectively), the observed strong frequency dependences of the χ'_{mol} and χ''_{mol} signals and the physically reasonable values of τ_0 also supported that these Co(II)-carbene complexes functioned as heterospin SMMs rather than spin glasses.[19] From the temperature at τ = 100 s in linear Arrhenius plots, furthermore, the blocking temperatures, T_{B}, were estimated to be 3.2, 4.8, and 3.3 K for $\mathrm{Co(X)_2(\mathbf{C1py})_4}$, X = $\mathrm{Cl^-}$ and $\mathrm{NCO^-}$, and $\mathrm{Co(Cl)_2(\mathbf{C1py'})_4}$, respectively, and that for $\mathrm{Co(NCO)_2(\mathbf{C1py})_4}$ exceeded a liquid helium temperature. At lower temperatures (<3.0 K), on the other hand, the τ values collected by the DC magnetization decay deviated downward from the extrapolation of the linear Arrhenius plot and become constant. The observed deviation suggests that in the low-temperature region (<3.0 K), the observed relaxation no longer follows the Arrhenius law and the temperature-independent pathway due to the RQT effect becomes dominant. From the constant values obtained by DC magnetization decay, the resonant magnetization tunneling times, τ_{Q}, for $\mathrm{Co(X)_2(\mathbf{C1py})_4}$, X = $\mathrm{NCS^-}$, $\mathrm{Cl^-}$, and $\mathrm{NCO^-}$, were estimated to be 6×10^2, 4×10^3, and 2×10^5 s, respectively, which corresponded to half-life times, $t_{1/2}$, of 3 min, 36 min, and 14 h, respectively. It is noted that the values of τ_{Q} could be determined by the DC magnetization decay in the temperature range of 3.0–1.9 K. The observed τ_{Q} might be due to the resonant quantum tunneling between $m_{\mathrm{s}} = \pm 9/2$. In the complexes, $\mathrm{Co(X)_2(\mathbf{C1py})_4}$, the U_{eff} values for $\mathrm{Co(NCS)_2(\mathbf{C1py})_4}$ and $\mathrm{Co(Cl)_2(\mathbf{C1py})_4}$ are close to each other while that for $\mathrm{Co(NCO)_2(\mathbf{C1py})_4}$ is larger. The noticeable finding is that the decays in the low temperature range due to τ_{Q} depend on the axial ligand and the τ_{Q} values increase in the order $\mathrm{Co(X)_2(\mathbf{C1py})_4}$, X = $\mathrm{NCS^-}$, $\mathrm{Cl^-}$, and $\mathrm{NCO^-}$, which is consistent with the order of the ligand field splitting in a spectrochemical series.[12]

The magnetic behaviors observed after irradiation of $\mathrm{Co(X)_2(\mathbf{C1py})_4}$ are reproducible. In annealing at 100 K, on the other hand, the observed SMM behaviors disappeared by chemical decomposition of carbene and returned to the magnetic behaviors before irradiation. This result clearly indicates that the magnetic interaction between the carbene center and the cobalt ion produces the heterospin SMM.

CONCLUSION

The magnetic behaviors observed in the AC and DC magnetic susceptibility experiments clearly indicated the formation of heterospin SMMs in frozen solutions. The heterospin SMM properties for $\mathrm{Co(X)_2(\mathbf{C1py})_4}$, X = $\mathrm{NCS^-}$, $\mathrm{Cl^-}$, and $\mathrm{NCO^-}$, strongly depended on the axial ligands, X. All physical values are summarized in Table 3 together with those for $\mathrm{Co(NCS)_2(\mathbf{C1Py})_4}$ and $\mathrm{Co(Cl)_2(\mathbf{C1py'})_4}$.

The physical values of $\mathrm{Co(Cl)_2(\mathbf{C1py'})_4}$ were consistent with those of $\mathrm{Co(Cl)_2(\mathbf{C1py})_4}$, suggesting that the molecular structure for $\mathrm{Co(Cl)_2(\mathbf{C1py})_4}$ is similar to that for $\mathrm{Co(Cl)_2(\mathbf{C1py'})_4}$ having an elongated octahedron. In this cobalt-carbene system, the temperature-independent DC magnetic relaxation could be measured to determine the values of quantum tunneling time τ_Q relating to the transverse anisotropic parameter, E.[1,21] The obtained τ_Q values for $Co(X)_2(\mathbf{C1py})_4$ depended on the axial ligands and increased in the order X = NCS^-, Cl^-, and NCO^-. The τ_Q values were estimated to be 6×10^2, 4×10^3, and 2×10^5 s for $Co(X)_2(\mathbf{C1py})_4$, X = NCS^-, Cl^-, and NCO^-, respectively. The τ_Q must be considered as a factor affecting U_{eff}; it reduces the U value to produce the U_{eff} value ($U > U_{eff}$). The U_{eff} values were 89, 91, and 130 K for $Co(X)_2(\mathbf{C1py})_4$, X = NCS^-, Cl^-, and NCO^-, respectively. Although the values for $Co(NCS)_2(\mathbf{C1py})_4$ and $Co(Cl)_2(\mathbf{C1py})_4$ were comparable, that for $Co(NCO)_2(\mathbf{C1py})_4$ was larger. Furthermore, the τ_Q also affected the hysteresis loop in the M versus H plot and the coercive force, H_c in the hysteresis loop increased with increasing τ_Q. Actually, the H_c values of 3.5, 7.0, and 20 kOe were obtained for $Co(X)_2(\mathbf{C1py})_4$, X = NCS^-, Cl^-, and NCO^-, respectively, and the order was in agreement with that for τ_Q.

In the cobalt-aminoxyl system, the change of U_{eff} depending on the axial ligand was also observed under similar conditions.[8c] (The U_{eff} values for $Co(X)_2(\mathbf{4NOpy})_4$, X = Br^-, NCS^-, and NCO^-, were 20, 31, and 50 K, respectively). The difference of the obtained U_{eff} values in $Co(X)_2(\mathbf{4NOpy})_4$ was considered to result from the change of the $|D|$ value by the axial ligands. In $Co(X)_2(\mathbf{4NOpy})_4$, on the other hand, the DC magnetic relaxations for the τ_Q values could not be followed by the using DC decay measurement and thus were fast. The τ_Q values for $Co(X)_2(\mathbf{4NOpy})_4$ were therefore considered to be smaller than those for the corresponding $Co(X)_2(\mathbf{C1py})_4$. The observed difference in τ_Q between the cobalt-carbene and the cobalt-aminoxyl systems suggest three important pieces of information for the construction of heterospin SMMs as follows: (1) the τ_Q was affected by not only the axial ligand but also the organic spin at the peripheral position in the 1:4 complex; (2) the magnetic interaction of carbene with the cobalt ion, which is larger than that of aminoxyl with the cobalt ion,[7] effectively increases the τ_Q value; and (3) the elongation of τ_Q leads to an increase in the U_{eff} value.[4a,c,d,22]

In this study on the heterospin SMM properties for the 1:4 Co(II)-carbene complexes having a simple molecular structure, we found that not only the axial ligand but also the organic spin at the peripheral position regulates the uniaxis magnetic anisotropy including the zfs parameters, $|D|$ and $|E|$, and strongly affects the heterospin SMM property. In $Co(X)_2(\mathbf{C1py})_4$, X = NCS^-, Cl^-, and NCO^-, especially, $Co(NCO)_2(\mathbf{C1py})_4$ had the characteristic SMM values of U_{eff} = 130 K with $\tau_Q = 2 \times 10^5$ s corresponding to $t_{1/2}$ of 14 h and showed a hysteresis loop with the H_c value of 20 kOe below 2.0 K. These values are fairly large compared with those for the metal clusters[2-4] reported in the literature.

■ ASSOCIATED CONTENT

Ⓢ Supporting Information. CIF files (CCDC-809474 and -809469 for $[Co(Cl)_2(\mathbf{D1py'})_4]$ and $[Co(NCO)_2(\mathbf{D1py})_4]$, respectively), the Vis. spectral change of **D1py** on photolysis (Figure S1), the plots of $\chi_{mol}T$ vs T (Figure S2), M_{mol} vs H (Figure S3), $\chi'_{mol}T$ and χ''_{mol} vs T (Figure S4), M/M_0 vs time (Figure S6), and ln τ vs T^{-1} (Figure S7) for $[Co(Cl)_2(\mathbf{C1py'})_4]$, and the plot of M vs time (Figure S5) and the values of τ and B (Table S1) for $Co(X)_2(\mathbf{C1py})_4$; **X** = Cl, NCS, and NCO. This material is available free of charge via the Internet at http://pubs.acs.org.

■ AUTHOR INFORMATION

Corresponding Author

*Phone: 81 92 642 6590. Fax 81 92 642 6590. E-mail: koga@fc.phar.kyushu-u.ac.jp.

■ ACKNOWLEDGMENT

This work was partially supported by “Nanotechnology Support Project” of the Ministry of Education, Culture, Sports, Science and Technology (MEXT), Japan.

■ REFERENCES

(1) Gatteschi, D.; Sessoli, R.; Villain, J. *Molecular nanomagnets*; OxfordUniversity Press: New York, 2006.

(2) (a) Miyasaka, H.; Clérac, R.; Wensdorfer, W.; Lecren, L.; Bonhomme, C.; Sugiura, K.; Yamashita, M. *Angew. Chem., Int. Ed.* **2004**, *43*, 2801. (b) Tasiopoulos, A. J.; Vinslava, A.; Wernsdorfer, W.; Abboud, K. A.; Christou, G. *Angew. Chem., Int. Ed.* **2004**, *43*, 2117. (c) Murugesu, M.; Habrych, M.; Wernsdorfer, W.; Abboud, K. A.; Christou, G. *J. Am. Chem. Soc.* **2004**, *126*, 4766. (d) Milios, C. J.; Inglis, R.; Vinslava, A.; Bagai, R.; Wernsdorfer, W.; Persons, S.; Perlepes, S. P.; Christou, G.; Brechin, E. K. *J. Am. Chem. Soc.* **2007**, *129*, 12505. (e) Lin, P.-H.; Burchell, T. J.; Ungur, L.; Chibotaru, L. F.; Wernsdorfer, W.; Murugesu, M. *Angew. Chem., Int. Ed.* **2009**, *48*, 9489. (f) Abbas, G.; Lan, Y. H.; Kostakis, G. E.; Wernsdorfer, W.; Anson, C. E.; Powell, A. K. *Inorg. Chem.* **2010**, *49*, 8067. (g) Riviere, E.; Donnio, B.; Voirin, E.; Rogez, G.; Kappier, J. P.; Gallani, J. L. *J. Mater. Chem.* **2010**, *20*, 7165. (h) Pajerowski, D. M.; Stamatatos, T. C.; Mukherjee, S.; Knowies, E. S.; Bencomo, M.; Meisei, M. V. V.; Christou, G. *Polyhedron* **2010**, *29*, 2462. (i) Moushi, E. E.; Lampropoulos, C.; Wernsdorfer, W.; Nastopoulos, V.; Chrostou, G.; Tasiopoulos, A. J. *J. Am. Chem. Soc.* **2010**, *132*, 16146.

(3) (a) Gatteschi, D.; Sessoli, R.; Cornia, A. *Chem. Commun.* **2000**, 725. (b) Benelli, C.; Cano, J.; Journaux, Y.; Sessoli, R.; Solan, G. A.; Winpenny, R. E. P. *Inorg. Chem.* **2001**, *40*, 188. (c) Oshio, H.; Hoshino, N.; Ito, T.; Nakano, M. *J. Am. Chem. Soc.* **2004**, *126*, 8805. (d) Moragues-Cánovas, M.; Helliwell, M.; Ricard, L.; Rivière, É.; Wernsdorfer, W.; Brechin, E.; Mallah, T. *Eur. J. Inorg. Chem.* **2004**, 2219. (e) Tancini, E.; Rodriguez-Douton, M. J.; Sorace, L.; Barra, A.-L.; Sessoli, R.; Cornia, A. *Chem.—Eur. J.* **2010**, *16*, 10482.

(4) (a) Lecren, L.; Wernsdorfer, W.; Li, Y. G.; Roubeau, O.; Miyasaka, H.; Clérac, R. *J. Am. Chem. Soc.* **2005**, *127*, 11311. (b) Chakov, N. E.; Lee, S.-C.; Harter, A. G.; Kuhns, P. L.; Reyes, A. P.; Hill, S. O.; Dalal, N. S.; Wernsdorfer, W.; Abboud, K. A.; Christou, G. *J. Am. Chem. Soc.* **2006**, *128*, 6975. (c) Milios, C. J.; Vinslava, A.; Wood, P. A.; Parsons, S.; Wernsdorfer, W.; Christou, G.; Perlepes, S. P.; Brechin, E. K. *J. Am. Chem. Soc.* **2007**, *129*, 8. (d) Milios, C. J.; Vinslava, A.; Wernsdorfer, W.; Moggach, S.; Parsons, S.; Perlepes, S. P.; Christou, G.; Brechin, E. K. *J. Am. Chem. Soc.* **2007**, *129*, 2754.

(5) (a) Osa, S.; Kido, T.; Matsumoto, N.; Re, N.; Pochaba, A.; Mrozinski, J. *J. Am. Chem. Soc.* **2004**, *126*, 420. (b) Rink, J.; Novitchi, G.; Van den Heuvel, W.; Ungur, L.; Lan, Y.; Wernsdorfer, W.; Anson, C. E.; Chibotaru, L. F.; Powell, A. K. *Angew. Chem., Int. Ed.* **2010**, *49*, 7583. (c) Baskar, V.; Gopal, K.; Helliwell, M.; Tuna, F.; Wernsdorfer, W.; Winpenny, R. E. P. *Dalton Trans.* **2010**, 4747. (d) Kajiwara, T.; Nakano, M.; Takahashi, K.; Takaishi, S.; Yamashita, M. *Chem.—Eur. J.* **2011**, *17*, 196.

(6) (a) Ishikawa, N.; Sugita, M.; Ishikawa, T.; Koshihara, S.; Kaizu, Y. *J. Am. Chem. Soc.* **2003**, *125*, 8694. (b) Ishikawa, N.; Sugita, M.; Wernsdorfer, W. *J. Am. Chem. Soc.* **2005**, *127*, 3650. (c) Pointillart, F.; Bernot, K.; Sessoli, R.; Gatteschi, D. *Chem.—Eur. J.* **2007**, *13*, 1602. (d) Lin, P.-H.; Burchell, T. J.; Ungur, L.; Chibotaru, L. F.; Wernsdorfer, W. *Angew. Chem., Int. Ed.* **2009**, *48*, 9489. (e) Jiang, S.-D.; Wang, B.-W.; Su, G.; Wang, Z.-M.; Gao, S. *Angew. Chem., Int. Ed.* **2010**, *49*, 7448.

(7) Koga, N.; Karasawa, S. *Bull. Chem. Soc. Jpn.* **2005**, *78*, 1384.

(8) (a) Karasawa, S.; Sano, Y.; Akita, T.; Koga, N.; Itoh, T.; Iwamura, H. *J. Am. Chem. Soc.* **1998**, *120*, 10080. (b) Karasawa, S.; Kumada, H.; Koga, N.; Iwamura, H. *J. Am. Chem. Soc.* **2001**, *123*, 9685. (c) Zhu, Z,; Karasawa, S.; Koga, N. *Inorg. Chem.* **2005**, *44*, 6004. (d) Karasawa, S.; Koga, N. *Inorg. Chem.* **2011**, *50*, 2055.

(9) (a) Karasawa, S.; Zhou, G.; Morikawa, H.; Koga, N. *J. Am. Chem. Soc.* **2003**, *125*, 13676. (b) Kanegawa, S.; Karasawa, S.; Nakano, M.; Koga, N. *Chem. Commun.* **2004**, 3590. (c) Kanegawa, S.; Karasawa, S.; Nakano, M.; Koga, N. *Bull. Chem. Soc. Jpn.* **2006**, *79*, 1372. (d) Tobinaga, H.; Suehiro, M.; Itoh, T.; Zhou, G.; Karasawa, S.; Koga, N. *Polyhedron* **2007**, *26*, 1905. (e) Karasawa, S.; Yoshihara, D.; Watanabe, N.; Nakano, M.; Koga, N. *Dalton Trans.* **2008**, 1418. (f) Kanegawa, S.; Karasawa, S.; Maeyama, M.; Nakano, M.; Koga, N. *J. Am. Chem. Soc.* **2008**, *130*, 3079. (g) Yoshihara, D.; Karasawa, S.; Koga, N. *J. Am. Chem. Soc.* **2008**, *130*, 10460.

(10) (a) Caneschi, A.; Gatteschi, D.; Lalioti, N.; Sangregorio, C.; Sessoli, R.; Venturi, G.; Vingdigni, A.; Rettori, A.; Pini, M. G.; Novak, M. A. *Angew. Chem, Int. Ed.* **2001**, *40*, 1760. (b) Ishii, N.; Okamura, Y.; Chiba, S.; Nogami, T.; Ishida, T. *J. Am. Chem. Soc.* **2008**, *130*, 24.

(11) (a) Bernot, K.; Bogani, L.; Caneschi, A.; Gatteschi, D.; Sessoli, R. *J. Am. Chem. Soc.* **2006**, *128*, 7947. (b) Bernot, K.; Pointillart, F.; Rosa, P.; Etienne, M.; Sessoli, R.; Gatteschi, D. *Chem Commun.* **2010**, 6458.

(12) Figgis, B. N.; Hitchman, M. A. *Ligand Field Theory and Its Application*; Wiley-VCH Publishers: New York, 2000.

(13) *SIR 92*; Altomare, A.; Burla, M. C.; Camalli, M.; Cascarano, M.; Giacovazzo, C.; Guagliardi, A.; Polidori, G. *J. Appl. Crystallogr.* **1994**, *27*, 435.

(14) *Crystal Structure 3.5.1*, Crystal Structure Analysis Package; Rigaku and Rigaku/MSC: The Woodlands, TX, 2000−2003.

(15) Morikawa, H.; Imamura, F.; Tsurukami, Y.; Itoh, T.; Kumada, H.; Karasawa, S.; Koga, N.; Iwamura, H. *J. Mater. Chem.* **2001**, 493.

(16) (a) Cotton, F. A.; Goodgame, D. M. L.; Goodgame, M. *J. Am. Chem. Soc.* **1961**, *83*, 4690.(b) Lever, A. B. P. *Inorganic Electronic Spectroscopy*, 2nd ed.; Elsevier: Amsterdam, The Netherlands, 1984. (c) Holland, J. M.; Kilner, C. A.; Thornton-Pett, M.; Halcrow, M. A. *Polyhedron* **2001**, *20*, 2829. (d) Kuzniarska-Biernacka, I.; Bartecki, A.; Kurzak, K. *Polyhedron* **2003**, *22*, 997.

(17) (a) Kahn, O. *Molecular Magnetism*; Wiley-VCH Publishers: Weinheim, Germany, 1993. (b) Rizzi, A. C.; Brondino, C. D.; Calvo, R.; Baggio, R.; Garland, M. T.; Rapp, R. E. *Inorg. Chem.* **2003**, *42*, 4409. (c) Pardo, E.; Ruiz-García, R.; Lloret, F.; Faus, J.; Julve, M.; Journaux, Y.; Novak, M. A.; Delgado, F. S.; Ruiz-Pérez, C. *Chem.—Eur. J.* **2007**, *13*, 2054. (d) Sarkar, M.; Aromí, G.; Cano, J.; Bertolasi, V.; Ray, D. *Chem.—Eur. J.* **2010**, *16*, 13833.

(18) (a) Bencini, A.; Benell, C.; Gatteschi, D.; Zanchini, C. *Inorg. Chem.* **1980**, *19*, 3027. (b) Faus, J.; Julve, M.; Lloret, F.; Real, J. A.; Sletten, J. *Inorg. Chem.* **1994**, *33*, 5535. (c) Caneschi, A.; Gatteschi, D.; Lalioti, N.; Sessoli, R.; Sorance, L.; Tangoulis, V.; Vindigni, A. *Chem.—Eur. J* **2002**, *8*, 286.

(19) Mydosh, J. A. *Spin Glasses, An Experimental Introduction*; Taylor and Francis: London, U.K., 1993.

(20) (a) Thomas, L.; Caneschi, A.; Barbara, B. *Phys. Rev. Lett.* **1999**, *83*, 2398. (b) Aubin, S. M. J.; Sun, Z.; Pardi, L.; Krzystek, J.; Folting, J.; Brunel, L.-C.; Rheingold, A. L.; Christou, G.; Hendrickson, D. N. *Inorg. Chem.* **1999**, *38*, 5329. (c) Hendrickson, D. N.; Christou, G.; Ishimoto, H.; Yoo, Y.; Brechin, E. K.; Yamaguchi, A.; Rumberger, E. M.; Aubin, S. M. J.; Sum, Z.; Aromi, G. *Polyhedron* **2001**, *20*, 1479.

(21) (a) Yoo, J.; Brechin, E. K.; Yamaguchi, A.; Nakano, M.; Huffman, J. C.; Maniero, A. L.; Brunel, L.-C.; Awaga, K.; Ishimoto, H.; Christou, G.; Hendrockson, D. N. *Inorg. Chem.* **2000**, *39*, 3615. (b) Kuroda-Sowa, T.; Lam, M.; Rheingold, A. L.; Frommen, C.; Reiff, W. M.; Nakano, M.; Yoo, J.; Maniero, A. L.; Brunel, L.-C.; Christou, G.; Hendrickson, D. N. *Inorg. Chem.* **2001**, *40*, 6469.

(22) Aubin, S. M. J.; Dilley, N. R.; Pardi, L.; Krzystek, J.; Wemple, M. W.; Brunel, L.-C.; Brian Maple, M.; Christou, G.; Hendrickson, D. N. *J. Am. Chem. Soc.* **1998**, *120*, 4991.